ARTICLES

Electronic structure of black sodalite

Otto F. Sankey, Alexander A. Demkov,* and Thomas Lenosky
Department of Physics and Astronomy, Arizona State University, Tempe, Arizona 85287-1504
(Received 18 November 1997)

The electronic structure of black sodalite, $Na_8(AlSiO_4)_6$, is determined in the local-spin-density approximation (LSDA). This structure has six Na atoms to compensate the six Al atoms, leaving two excess Na atoms. A band-gap electronic state is induced in the wide oxide gap by the excess sodium, and has ''particle in a box'' behavior. Magnetic orderings of these gap states are studied. Analytic models show that an antiferromagnetic ordering is lowest in energy in the LSDA. A self-consistent LSDA calculation shows the system to change from a metal to an antiferromagnetic insulator when spin orderings are allowed. Hopping and Hubbard-U parameters are estimated, and the many-body correlated Hubbard model is solved using a constrained path Monte Carlo technique, which again predicts the system to be antiferromagnetic with a T_c of order 50 K. [S0163-1829(98)00723-1]

I. INTRODUCTION

Zeolites are open framework structures, which generally contain large polyhedral cages of tetrahedrally bonded atoms connected to each other by channels. The tetrahedral atom (T atom) is usually Si and is surrounded by four oxygen atoms. It is common that the element Al is substituted for some of the Si atoms. In these aluminosilicates, an additional cation (e.g., Na) is incorporated interstitially within a cage or channel. Its donated electron resides near an Al site to satisfy the bonding requirements of a tetrahedral framework.

The cavities of the material can be occupied by guest atoms, ions, or molecules (such as water), and allow considerable freedom of movement. These materials permit ion exchange and reversible dehydration. As such, zeolites play a major role in petrochemical catalysis, and also are widely used in radioactive waste storage, water treatment, gas separation and purification, and animal feed supplements—all because of their exceptional abilities for ion exchange and sorption.[1]

Zeolite frameworks offer a unique opportunity for creating new three-dimensional arrays of clusters,[2] or supralattices,[3–6] i.e., artificial periodic lattices of clusters or ''quantum dots'' of semiconducting (or other) materials whose dimensionality and electronic properties can be partially controlled.[7] There are three basic bonding schemes[6,8] for the incorporation of clusters in zeolites: *chemiencapsulation, physiencapsulation,* and *charge-transfer encapsulation.* Chemiencapsulation of a cluster occurs when the cluster forms covalent bonds with the host matrix. Physiencapsulation is more common and is the case in which the molecule in the cage partially or completely fills the void, and the interstitial molecule is only very weakly bound to the framework. The final category is the case of charge encapsulation in which the cluster in the cavity is charged due to charge transfer between it and the framework.

In this paper we study the electronic properties of a prototypical charge-transfer encapsulated cluster—a periodic array of Na_4^{+3} clusters[9] in sodalite. This actual material is known as black sodalite, $Na_4^{3+}(AlSiO_4)_3^{3-}$. In particular we investigate the formation of magnetic electronic states in this system, i.e., antiferromagnetic and ferromagnetic states. The Na_4 cluster forms a narrow band in the wide aluminosilicate band gap, and this band, which is nominally metallic, is greatly influenced by many-body electron effects, due to the large spatial separation between Na_4^{3+} clusters. We use the local-spin-density approximation to examine these magnetic states in this mean-field-like theory. From these calculations we are able to extract model parameters for a many-body treatment of a Hubbard-like model.

Alkali-metal clusters in zeolites and their electronic properties have been under continuous investigation since the late 1960s.[9,10] It was noticed that the absorption of alkali-metal atoms by zeolites causes simultaneously the introduction of excess electrons and extra cations into the zeolite. The excess electron is said to be solvated by the counter-ion trap. More information and the latest references can be found in two recent reviews.[11,12] Magnetic properties of sodium and potassium clusters in supercages of zeolite A have been studied experimentally by Nozue *et al.*[13] and by Kodaira *et al.*[14] Hubbard models were recently applied to study magnetic properties of potassium doped zeolite A,[15] and Na_4^{3+} clusters in the sodalite cage of zeolite Y by Ursenbach *et al.*[16] Of particular relevance to the current paper is the pioneering work on Na_4^{3+} clusters in sodalite, which were studied both experimentally and theoretically by the Santa-Barbara group.[17–20] The optical-absorption spectrum was measured and calculated.[17,18] The theoretical description was later refined by Monnier *et al.*[19] and by Blake *et al.*[20]

It has only been recently that density-functional theory has been applied to zeolites due to the large unit cells and the complexity of these materials. A recent review can be found in Ref. 7. Trave *et al.*[21] have studied microclusters of III-V semiconductors in sodalite, which is an example of a che-

miencapsulated system. Demkov *et al.*[8,7] have investigated Si microclusters in silaceous sodalite as a model system, and have studied other complex oxides.[22] Of particular relevance to the present work is that of Filippone *et al.*,[23] who performed LDA calculations of sodalite. They performed a comprehensive study of this material, including optimization of the geometrical structure and vibrational modes. An examination of the material was made with different guest species, and they investigated the electronic density of states. Many silica polymorphs have been studied using density-functional theory by the Missouri group.[24] Other zeolites such as offretite[25] have been studied using density-functional methods, and density-functional theory has been applied to complex minerals.[26,27] Other electronic-structure methods have been applied to zeolites and examples can be found in Ref. 28 and Ref. 29.

Part of the motivation of this work is a recent report of Srdanov *et al.*,[30] who studied the NMR spectra of Na in black sodalite. They find clear evidence from the temperature dependence of the susceptibility that the system transforms from a paramagnetic state to an antiferromagnetic state below the transition temperature of 55 K. They note that this system provides the first example of an *s*-electron antiferromagnet.

In this paper we will study the electronic properties of black sodalite $Na_8(AlSiO_4)_6$ using local-spin-density-functional theory. To our knowledge, this is the first application of spin-density-functional theory to a zeolite. We will first simplify the system theoretically, and construct an analytical model with parameters, then determine the type of magnetic orderings of the electrons that are possible in this system. The values of the parameters that give each type of ordering are established. Next, a self-consistent solution of the LSDA is found and the system is shown to be antiferromagnetic. This result is found to be consistent with the analytical model. Finally, a Hubbard model is solved that properly includes the many-body effects and electron correlations.

II. STRUCTURE OF SODALITE

Sodalite (SOD) (Ref. 31) is probably the simplest of the zeolite framework structures. The building block of the sodalite structure is the β or kelvin cage. The β cage shown in Fig. 1 is a truncated octahedron, with 24 vertices and 14 faces. The faces are six square faces and eight hexagonal faces. At each of the vertices is a *T* atom (tetrahedral Si or Al) and oxygen atoms bridge the *T* atoms in puckered off-line positions. By stacking the β cages together at the square faces, a body-centered-cubic (bcc) array of β cages is formed that is the sodalite framework. Other zeolite structures can be formed by connecting the *T* atoms of different cages through additional oxygen bridge atoms across hexagonal faces or square faces to form faujasite (FAU) or Linde-type A (LTA), respectively.

It was noted very early[32] that the interaction of Na vapor with a synthetic zeolite caused the sodalite to color and darken. The interpretation is that excess Na atoms enter into the cages to form Na_4^{3+}, which produce localized electronic states (similar to color centers) in the lattice. These paramagnetic clusters are isolated from each other. An electron-spin resonance (ESR) signal of the Na_4^{3+} cluster[33] shows a 13-peak hyperfine structure indicative that an unpaired electron is shared over the four Na atoms.

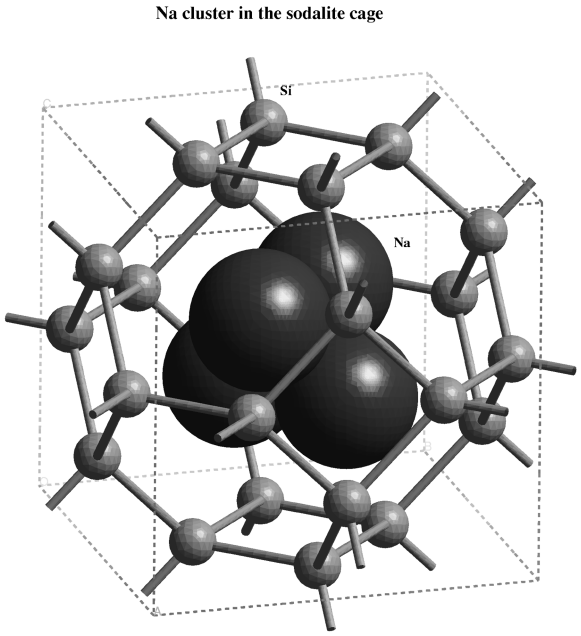

FIG. 1. A ball and stick model of a single β cage in black sodalite. The four atoms in the center of the cage are Na atoms, and are not part of the β cage, but are the guest atoms in black sodalite. The cage framework *T* atoms are Si alternating with Al (or just Si in silaceous sodalite.) Oxygen atoms (not shown) lie between the *T* atoms in bent bridging sites.

The material we study here contains a Na_4^{3+} cluster in each of the sodalite cages. A Na_4 cluster is normally incorporated in the sodalite cage along with a central anion to form the material $Na_4(AlSiO_4)_3X$, where *X* is an anion (e.g., Cl). Smeulders *et al.*[33] have found that by exposing the material to Na vapor, the anion can be removed and black sodalite $Na_4^{3+}(AlSiO_4)_3^{3-}$ is formed. Samples of black sodalite have been prepared by Srdanov[18] using a similar Na vapor technique.

We perform electronic-structure calculations on two different sodalite structures—silica sodalite and black sodalite. The first structure, silica sodalite $(SiO_2)_{12}$, is that of the pure SiO_2 form of sodalite. This material has no aluminum and no sodium cations, and the Bravais lattice is body-centered-cubic since all *T* atoms are of one type, namely Si. It was first synthesized in 1985 by Bibby *et al.*,[34] who named it silica-sodalite, and Richardson *et al.*[35] performed further work. The material is prepared using a nonaqueous solvent (ethylene glycol or propanol). A crystallographic description of the structure, which has space group $Im\bar{3}m$, is given in Table I.

The second structure is that of black sodalite, which is an aluminosilicate with an even mix of Si and Al atoms. The number of *T* atoms per primitive cell is twice that of silica sodalite and the Bravais lattice expands to a simple-cubic lattice of space group $P\bar{4}3n$. The structural parameters for black sodalite, $Na_8(AlSiO_4)_6$, are shown in Table II. The coordinates were determined by Pauling[36] and later refined by Loïns *et al.*[37] This structure is, however, determined from

TABLE I. The structural parameters of all silicon sodalite, $(SiO_2)_{12}$. The parameters are from Bibby *et al.* (Ref. 34) and Richardson *et al.* (Ref. 35). Space group $Im\bar{3}m$ (no. 229), $a=8.830$ Å. $d_{\text{Si-O}}=1.587$ Å, $\theta_{\text{Si-O-Si}}=159.7°$.

Atom	Site	Position
12 Si	12*d*	$(\frac{1}{4},\frac{1}{2},0)$, etc.
24 O	24*h*	$(0,y,y)$, etc., $y=0.6474$

that of chlorinated sodalite, $Na_4(AlSiO_4)_3Cl$, in which the four Na atoms, which form a tetrahedron inside the β cage, are surrounding a Cl^- atom. We have assumed, therefore, little relaxation of the Na in the absence of the the anion. This assumption is in line with the recent x-ray analysis of black sodalite by Srdanov.[38]

In order to make comparisons of the electronic structure of silica sodalite more transparent, we can describe the bcc silica-sodalite as having a larger unit cell in the simple-cubic $P\bar{4}3n$ space group. In Table III we give the coordinates of silica-sodalite in this space group. The Brillouin zone of the structure of Table III is then identical to the Brillouin zone for black sodalite in Table II, making band-structure comparisons between the two clear.

III. COMPUTATIONAL DETAILS

In the self-consistent results given below, we will use the local-spin-density approximation (LSDA) for systems with a spin density, and the local-density approximation (LDA) for an unpolarized spin charge density. The calculations are done within the pseudopotential approximation, which is a device to replace each atom by a pseudoatom that has only the valence electrons of the system. We use norm-conserving separable forms for the semilocal pseudopotential.[39] The soft pseudopotentials are generated by the Kerker-Troullier-Martins[40] scheme. The pseudoatom wave functions are matched to the all-electron wave function at a radius R_{match}. The values chosen for R_{match} (in Bohr units) are 1.5 for oxygen *s* and *p* states, 1.75 and 2.1 for both Si and Al *s* and *p* states, respectively, and 3.0 for the Na *s* state. Convergence in reciprocal space is limited by the strength and size of the oxygen pseudopotential, since it is the strongest and most compact.

We use the local atomic orbital sp^3 basis on each of the atoms.[41] The atomic orbitals are written as linear combinations of Bloch orbitals, and then this is decomposed into plane waves. The matrix elements, charge density, and the solution of Poisson's equations are then conveniently evaluated using fast Fourier transforms in reciprocal space. The Hamiltonian matrix, since it is in a local orbital basis, remains relatively small compared to a full plane-wave calculation. We have performed limited tests using a full plane-wave basis and have determined that the results for the bands (at least for the unpolarized case) were very similar to those generated using a local basis, and thus we were not compelled to continue these far more lengthy calculations. In addition, we make use of the symmetry of the problem and use a single special *k* point[42] $[(\pi/2a)(111)$, where *a* is the cubic lattice constant] in the irreducible wedge of the Brillouin zone.

TABLE II. The structural parameters of black sodalite, $Na_8(AlSiO_4)_6$. The parameters are from Pauling (Ref. 36) and Löns *et al.* (Ref. 37). Space group $P\bar{4}3n$ (no. 218), $a=8.881$ Å. $d_{\text{Si-O}}=1.63$ Å, $d_{\text{Al-O}}=1.73$ Å, $d_{\text{Na-O}}=2.35$ Å, $d_{\text{Na-Na}}=4.46$ Å, *T*-O-*T* angle $=138.3°$.

Atom	Site	Position
6 Si	6*d*	$(\frac{1}{4},0,\frac{1}{2})$, etc.
6 Al	6*c*	$(\frac{1}{4},\frac{1}{2},0)$, etc.
24 O	24*i*	(x,y,z), etc., $x=0.1401$, $y=0.4385$, $z=0.1487$
8 Na	8*e*	(x,x,x), etc., $x=0.1777$

TABLE III. The structural parameters of all silicon sodalite, $(SiO_2)_{12}$, in a simple-cubic Bravais lattice. The geometry is identical to that of Table I, but is described here as a simple-cubic rather than body-centered-cubic lattice. Space group pseudo-$P\bar{4}3n$ (no. 218), $a=8.830$ Å. $d_{\text{Si-O}}=1.587$ Å, $\theta_{\text{Si-O-Si}}=159.7°$.

Atom	Site	Position
6 Si	6*d*	$(\frac{1}{4},0,\frac{1}{2})$, etc.
6 Si	6*c*	$(\frac{1}{4},\frac{1}{2},0)$, etc.
24 O	24*i*	(x,y,z) etc., $x=0$, $y=z=0.6474$

In order to determine the spin polarization, we use the local-spin-density approximation (LSDA).[43] Let the electron density, $n(\vec{r})$, be written in terms of its spin-up and spin-down components, $n=n_\uparrow+n_\downarrow$. The total exchange and correlation energies are given by $E_{\text{xc}}[n_\uparrow,n_\downarrow]=\int d^3r[\epsilon_x(n_\uparrow,n_\downarrow)+\epsilon_c(n_\uparrow,n_\downarrow)]n(\vec{r})$. A paramagnetic (unpolarized) system has equal up and down spin densities, $n_\uparrow=n_\downarrow$. However, for a magnetic system, the spins polarize and a convenient measure is the spin polarization parameter ξ, where $\xi=(n_\uparrow-n_\downarrow)/n$. The exchange energy of a paramagnetic free electron gas is $\epsilon_x^P(n)=-3/4e^2(3/\pi)^{1/3}n^{1/3}$, while for a completely polarized ferromagnetic gas it is $\epsilon_x^F(n)=2^{1/3}\epsilon_x^P(n)$. In the LSDA, the exchange energy $\epsilon_x(n_\uparrow,n_\downarrow)$ of an arbitarily spin polarized gas is given by[43]

$$\epsilon_x(n_\uparrow,n_\downarrow)=\epsilon_x(n,\xi)=\epsilon_x^P(n)+[\epsilon_x^F(n)-\epsilon_x^P(n)]f(\xi).$$

The function $f(\xi)$ $(0\leqslant f\leqslant 1)$ interpolates between the paramagnetic and ferromagnetic limits, and is

$$f(\xi)=\frac{(1+\xi)^{4/3}+(1-\xi)^{4/3}-2}{2^{4/3}-2}.$$

The correlation energy is assumed to interpolate in the same manner, and we use the correlation energy ϵ_c of Ceperley[44] (as parametrized by Perdew *et al.*).

IV. SIMPLIFIED LSDA MODEL OF SPIN-POLARIZED SODALITE

To gain an understanding of the possible spin polarizations in black sodalite, we present in this section a simple *analytical model* of the LSDA theory, which will be useful in seeing the full range of possible solutions, the limitations of

the LSDA, and will be useful in interpreting the self-consistent results of the next section. This analytical model is useful for understanding not only black sodalite, but it may also be generalizable under certain assumptions to other zeolite systems that have excess cations in cages. In the next section, we will present the results of the fully self-consistent numerical LSDA calculation for black sodalite.

We assume that the excess electron trapped in the sodalite cage can be approximated by an s state in a spherical box of radius ''a_0,''

$$\psi_0 = A j_0(kr), \tag{1}$$

where j_0 is the spherical bessel function, $k=\sqrt{2mE/\hbar^2}=\pi/a_0$, and A is a normalization constant. As will be seen from Sec. V, such a wave function represents a reasonable (but incomplete) approximation for black sodalite.

Black sodalite is a bcc stacking of sodalite cages. We consider a simple-cubic lattice with two cages ($i=1$ and 2) at basis vectors $\vec{b}_1=(000)$ and $\vec{b}_2=(a/2)(111)$, respectively. We assume a nearest-neighbor model in which an electron in each of these cages can tunnel or ''hop'' to eight nearest neighbors with hopping integral $-t$.

For simplicity, we only consider the exchange interaction in this model, and neglect the correlation energy. (Note that this is not Hartree-Fock, since we use the LDA exchange functional, which will reduce to the Hartree-Fock limit only in the limit of the uniform electron gas.) To justify the neglect of correlation, we may make an estimate of relative importance of exchange and correlation to be certain that the exchange is the dominant effect. First we estimate ϵ_x and ϵ_c for the entire black sodalite system, including framework atoms and the Na guest interstitial atoms. The 194 valence electrons of $Na_8(AlSiO_4)_6$ in the volume of the cubic cell gives an average electron number density of $n=0.275/\text{Å}^3$. At this value average of n, $|\epsilon_x|\approx 5|\epsilon_c|$. Another point of view is to ignore the framework and consider only a single Na atom in a cage of approximately 3.5 Å in diameter, where we obtain an average n of $0.006/\text{Å}^3$, and $|\epsilon_x|\approx 3|\epsilon_c|$. This latter estimate is probably more appropriate for the current problem. However, in either case the exchange energy is expected to be dominant, and neglecting the correlation energy is expected to be a sensible approximation.

We construct a model LSDA Hamiltonian, and take

$$E = -t\Sigma_{i,\vec{l}}\Sigma'_{i',\vec{l}'}[\hat{a}_i^\dagger(\vec{l})\hat{a}_{i'}(\vec{l}')+\hat{a}_{i'}^\dagger(\vec{l}')\hat{a}_i(\vec{l})] + \Sigma_{i,\vec{l}}Un_i(\vec{l})n_i(\vec{l}) - K\Sigma_{i,\vec{l}}(n_i(\vec{l}))^{4/3}[1+(2^{1/3}-1)f(\xi)]. \tag{2}$$

The first term is the hopping or kinetic energy term, where the sum over i',l' is restricted to first neighbors of the basis cage i in the unit cell $\vec{l}$. The second term is a Hartree on-site (or Hubbard-like) interaction, and the final term is the exchange energy, which has strength K. The exchange energy being proportional to $n\times n^{1/3}$ (or $n^{4/3}$) and $\epsilon^F(n)=2^{1/3}\epsilon^U(n)$ has been used.

We let $\psi_0(k|\vec{r}-\vec{l}-\vec{b}_1|)$ and $\psi_0(k|\vec{r}-\vec{l}-\vec{b}_2|)$ be the wave functions of Eq. (1) centered in cage 1 and cage 2, respectively, in the cell at $\vec{l}$. We replace the Brillouin zone sum, by a single special k point, $\vec{k}_0=(\pi/2a)(111)$, which is the special k point of a simple-cubic lattice. The Bloch states at this k point are $\psi_{\vec{k}_0,\sigma}(\vec{r})=[a\phi_1(\vec{k}_0)+b\phi_2(\vec{k}_0)]\sigma$, where $\phi_i(\vec{k}_0)=(1/\sqrt{N})\Sigma e^{i\vec{k}_0\cdot(\vec{l}+\vec{b}_i)}\psi_0(k|\vec{r}-\vec{l}-\vec{b}_i|)$, and the spin state σ is either up or down. Without loss of generality, we choose the phases for this bcc system so that a and b are real, and write the wave-function expansion in terms of a mixing angle θ,

$$\psi_{\vec{k}_0,\sigma}(\vec{r})=[\cos(\theta)\phi_1(\vec{k}_0)+\sin(\theta)\phi_2(\vec{k}_0)]\sigma. \tag{3}$$

For normalization purposes, we assume the overlap between neighbors is small so that $\cos^2\theta+\sin^2\theta=1$.

For a simple paramagnetic system, each electron will be found with equal probability in each of the two cages ($i=1$ or 2), which corresponds to $\theta=45°$. However, the competition between the kinetic and exchange interactions may yield magnetic states where up and down spin densities are not equal. There are two excess Na atoms per unit cell of $Na_8(AlSiO_4)_6$, and these excess Na atoms contribute their electrons to the two cages of the unit cell. The state of the first electron is determined by θ_1,σ_1, and the second electron by θ_2,σ_2. We now write the expression for the total energy per unit cell in terms of these two angles (θ_1 and θ_2) for the three possible choices of the spin quantum numbers. The three choices are (i) $\sigma_1=\alpha$, $\sigma_2=\alpha$ (ferromagnetic), (ii) $\sigma_1=\alpha$, $\sigma_2=\beta$, and $\theta_1,\theta_2\neq 45°$ (antiferromagnetic), and (iii) $\sigma_1=\alpha$, $\sigma_2=\beta$, $\theta_1=\theta_2=45°$ (paramagnetic). The kinetic (hopping) energy at a given $\vec{k}$ is given for all cases as

$$E_{\text{hop}}(\vec{k}) = -8t\cos(k_xa/2)\cos(k_ya/2) \times\cos(k_za/2)2[\cos(\theta_1)\sin(\theta_1)+\cos(\theta_2)\sin(\theta_2)], \tag{4}$$

which simplifies for $\vec{k}=\vec{k}_0$ to

$$E_{\text{hop}}(\vec{k}_0) = -4\sqrt{2}t[\cos(\theta_1)\sin(\theta_1)+\cos(\theta_2)\sin(\theta_2)]. \tag{5}$$

We now consider the total energy per cell for each of the three cases in turn. We work in energy units of t, and thus have rescaled variables to reduce the number of parameters in the problem.

We first examine the ferromagnetic case (i). The two Bloch states must be orthogonal, which gives the condition that $\theta_2=\theta_1\pm\pi/2$. A change of mixing angle of $\pi/2$ changes the bonding state into an antibonding state (and vice versa). The net kinetic energy then becomes zero. The other contributions have $n_in_i=1$, $n_i^{4/3}=1$, and $f(\xi)=1$. We obtain

$$E^F(\theta_1,\theta_2=\theta_1\pm\pi/2)/t = 2(U/t-2^{1/3}K/t). \tag{6}$$

Note that the angle θ_1 drops out.

We next consider the antiferromagnetic (AF) state (ii), where one electron per unit cell has spin up, and the other spin down, but the charge density for a given spin is not equally distributed over the two cages. The two wave functions are already orthogonal due to spin, and there is no explicit relationship between θ_1 and θ_2. The energy per cell for this case is

$$E^{\mathrm{AF}}(\theta_1,\theta_2) = -4\sqrt{2}[\cos(\theta_1)\sin(\theta_1)+\cos(\theta_2)\sin(\theta_2)] + U/t[(\cos^2\theta_1+\cos^2\theta_2)^2 + (\sin^2\theta_1+\sin^2\theta_2)^2] - K/t\{(\cos^2\theta_1+\cos^2\theta_2)^{4/3} \times[1+(2^{1/3}-1)f(\xi_1)]+(\sin^2\theta_1+\sin^2\theta_2)^{4/3} \times[+(2^{1/3}-1)f(\xi_2)]\}, \quad (7)$$

where $\xi_1=[\cos^2(\theta_1)-\cos^2(\theta_2)]/[\cos^2(\theta_1)+\cos^2(\theta_2)]$, and $\xi_2=[\sin^2(\theta_1)-\sin^2(\theta_2)]/[\sin^2(\theta_1)+\sin^2(\theta_2)]$. We know of no analytic solution of this equation, so we minimize this expression numerically with respect to θ_1 and θ_2 for different choices of the parameters U/t and K/t.

The paramagnetic case is a special case of the antiferromagentic system above, but where $\theta_1=\theta_2$, and the spin polarizations ξ_1 and ξ_2 are zero. The energy per cell is

$$E^P(\theta_1)/t = E^{\mathrm{AF}}(\theta_1,\theta_2=\theta_1)/t = -8\sqrt{2}\cos\theta_1\sin\theta_1 + 4U/t(\cos^4\theta_1+\sin^4\theta_1) - 2^{4/3}K/t(\cos^{8/3}\theta_1 + \sin^{8/3}\theta_1). \quad (8)$$

It is easy to see that the paramagnetic case allows two possible charge densities—one corresponds to equal charge densities in the two cages, and the second corresponds to a charge-density wave in which the symmetry is broken and one cage has an excess charge compared to the other. The equal charge-density case occurs when $\theta_1=\pi/4=45°$, so that the charge density in the first cage is $\cos^2\theta=1/2$, and the charge density in the other cage is $\sin^2\theta=1/2$. This amounts to the usual bonding orbital wave function of $\psi=1/\sqrt{2}(\phi_1+\phi_2)$.

The charge-density-wave situation occurs when $\theta\neq 45°$. We let $\theta=\pi/4+\delta$, and expand the energy in Eq. (8) to second order in δ and to find $E(\delta)=-4\sqrt{2}+2U/t-2K/t+(8\sqrt{2}+8U/t-16/9K/t)\delta^2$. The curvature changes from concave upward to concave downward at the critical value of $(K/t)_{\mathrm{crit}}=\frac{9}{2}(\sqrt{2}+U/t)$. For K/t values larger than $(K/t)_{\mathrm{crit}}$, the charge-density wave forms, and the two cages have inequivalent densities even in the paramagnetic case. The function $E^P(\theta)-E^P(45°)$ determined by Eq. (8) for two values of K/t is shown in Fig. 2. The double minimum curve is the signature of the charge-density wave.

We may make an estimate of the relative size of K and U from our approximate wave function ψ_0 [see Eq. (1)]. The Hartree repulsion U is given by

$$U=e^2\int_{\mathrm{sphere}}^{\mathrm{radius}\ a_0}\frac{|Aj_0(\pi r/a_0)|^2|Aj_0(\pi r'/a_0)|^2}{|\vec{r}-\vec{r}'|}d^3r\,d^3r', \quad (9)$$

which numerically gives $U\approx 26$ eV Å$/a_0$, while the exchange integral is

$$K=\frac{3e^2}{4}\left(\frac{3}{\pi}\right)^{1/3}\int_{\mathrm{sphere}}^{\mathrm{radius}\ a_0}\left(\left|Aj_0\left(\frac{\pi r}{a_0}\right)\right|^2\right)^{4/3}d^3r = 8.8\ \text{eV Å}/a_0. \quad (10)$$

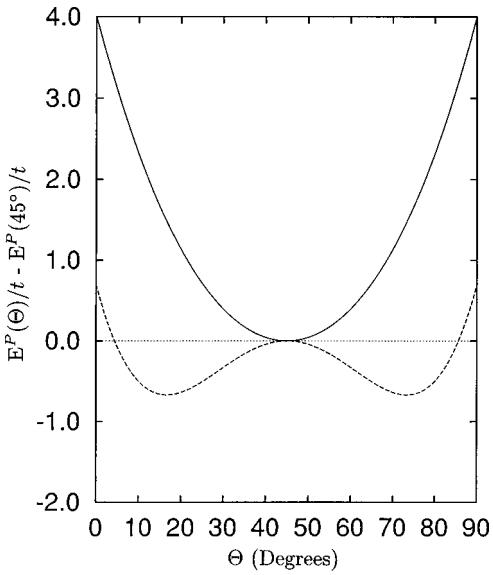

FIG. 2. A plot of $E^P(\theta)-E^P(45°)$ for a paramagnetic system with and without a charge-density wave. The single minimum curve is for $K/t=1/2(K/t)_{\mathrm{crit}}$, and yields a minimum at 45° indicating equal charge densities in the two cages of the unit cell. The double minimum curve is for $K/t=1.5(K/t)_{\mathrm{crit}}$ and exhibits a charge-density wave where the minimum occurs at $\theta\neq 45°$, indicating unequal charge densities in the two cages.

We will see in the next section that $t\ll U,K$, and thus neglecting t shows that the criterion for the charge-density wave is $K>\frac{9}{2}U$, which using our estimate for K and U gives 8.8 eV Å$/a_0>117$ eV Å$/a_0$, which is never satisfied. Thus charge-density waves are unlikely in sodalite (at least within this model) and we no longer include this possibility.

We now search for the minimum energy configuration for the ferromagnetic system [Eq. (6)], the antiferromagnetic system [Eq. (7)], and the paramagnetic system [Eq. (8)]. We restrict our minimization to cases in which there is no charge-density wave so that the total densities in the two cages are equal, leading to a Hartree contribution of $2U$. Thus U is effectively removed from the problem, and different spin polarizations occur in the two cages because of the interplay between exchange and kinetic energies (i.e., between the K and t parameters).

By comparing Eqs. (6) and (8), it is easy to show that the phase boundary between ferromagnetic and paramagnetic systems is given by $K/t>2\sqrt{2}/(2^{1/3}-1)=10.88$ with the ferromagnetic state favored for large values of K/t. The ferromagnetic state, however, is never found to be the absolute ground state. A numerical minimization of the antiferromagnetic energy [Eq. (7)] is always found to be lower than the ferromagnetic state. The results for the minimum energy for all three possible states are shown in Fig. 3. We plot the energy $(E-2U)/t$ versus the ratio K/t. We see that the ferromagnetic energy crosses the paramagnetic term at $K/t=10.88$ as discussed above. More importantly, we find that the absolute minimum energy state is paramagnetic for small K/t, and for $K/t>1.59$ it is antiferromagnetic.

There are two immediate conclusions that we can draw. The first is that this analysis predicts that if the assumptions of this model are met, then it is very easy for an antiferromagnetic spin density to form in black sodalite. We come to

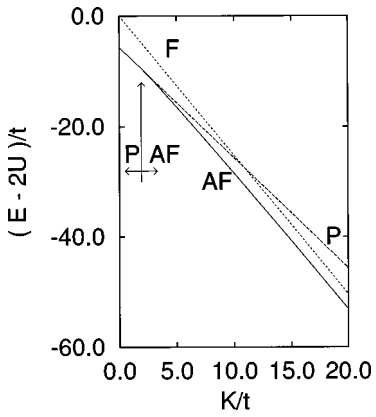

FIG. 3. A plot of the minimum total energy E, $(E-2U/t)$ as a function of K/t for the three possible spin states: ferromagnetic (F), antiferromagnetic (AF), and paramagnetic (P). The model used is the simplified LSDA model. The lowest energy state is paramagnetic for low K/t but switches to antiferromagnetic for larger values of K/t. The transition region is indicated by the arrows. The spin densities are determined by allowing a periodic spin density of the two cages in the sodalite unit cell.

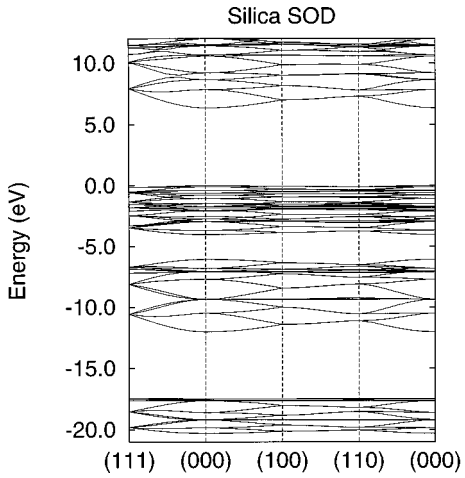

FIG. 4. Band structure of paramagnetic silica sodalite, $(SiO_2)_{12}$. The valence-band maximum is at zero energy and the conduction bands begin around 6 eV. The simple cubic unit cell is used, and the k points along the abscissa are in units of π/a. The lowest several conduction states have wave functions spread over the framework, and have little amplitude inside the β cages.

this conclusion by approximating K using Eq. (9) with $a_0 \approx 4$ Å, which gives $K \approx 2$ eV, so that the antiferromagnetic transition will occur for $t < K/1.59 \approx 1.26$ eV. A t value of 1.26 eV is of the same order (within a factor of 2 or 3) as that of a covalent bond, such as between two Si atoms in the diamond structure. We will estimate ''t'' in the next section when we perform self-consistent LDA calculations, but one would certainly expect tunneling (or hopping) of an electron from one cage to another in sodalite to be less than that of the usual covalent bond, and thus the system should be antiferromagnetic.

The second conclusion is that the model has uncertainties for large values of K/t, which is in the regime we expect to be in. The reason is that *fractionally*, the energy difference between all three spin states is becoming small. For example, at $K/t = 10$, the fractional energy difference between all three spin states is only about 10%. Thus flaws in the model may upset the balance between the energetics of these three possible spin systems.

V. SELF-CONSISTENT LDA AND LSDA RESULTS

We now give the results of the self-consistent density-functional calculations. We first discuss the electronic band structure and total energy of silica sodalite and black sodalite using the local-density approximation, which does not allow for spin polarization. Shown in Fig. 4 is the band structure for silica sodalite $(SiO_2)_{12}$ in the simple-cubic lattice (see Table III). The doubling of the unit cell (from the bcc cell of Table I) allows a clearer comparison with the band structure of black sodalite. The top of the valence band is derived from oxygen p-like states and is arbitrarily set to zero energy, and the conduction band begins about 6 eV. Thus the band gap is approximately 6 eV. When we examine the first several wave functions of the conduction band at the Γ point $[k=(000)]$, we find that the wave functions are localized on the SiO_2 framework, and not in the cavities of the β cages. A clue that this is the case can also be seen by the high degeneracy of the bands at the L point $[k=(\pi/a)(111)]$. Thus even though one would expect particle-in-a-box states to exist for the β cage, these states are not near the conduction-band edge, and likely lie high in energy above the lowest several conduction-band states.

We now examine the band structure for black sodalite, $Na_8(AlSiO_4)_6$. The band structure for the paramagnetic system is shown in Fig. 5(a). The valence bands of the underlying aluminosilicate are those bands of negative energy, and again the top of the aluminosilicate bands is defined to have zero energy. We see the formation of a pair of bands that are centered at about $+3.6$ eV, which did not exist in the silica sodalite, $(SiO_2)_{12}$. These bands are generated by the ''particle-in-a-box'' states. Figure 6 shows a constant charge-density contour of the lowest energy band state at ~ 3.1 eV at the Γ point. The large ''spherical'' charge density in the center of the β cage is the particle-in-a-box state represented analytically by Eq. (1). However, Fig. 6 shows appreciable charge density localized around the oxygen atoms decorating the framework, which are seen in the figure as ''spheroidal blobs.'' Thus the particle-in-a-box state is better described as a particle in a box hybridized with framework oxygen atoms.

The particle-in-a-box state did not appear in silaceous sodalite, so the presence of the β cage alone is not enough to generate the particle-in-a-box state near the conduction-band edge. The attractive Coulomb potential of Na is required to drive the average potential of the cage to lie near the band gap. The Na atoms of black sodalite contribute two excess electrons, and these two excess electrons fill the lowest band in the pair of ''particle-in-a-box'' bands. Since these two bands are capable of containing four electrons (including spin), the system is predicted to be metallic.

A close up view of the ''particle-in-a-box'' bands is shown in Fig. 5(b). The double degeneracy that exists along the line running from $(\pi/a)(100)$ to $(\pi/a)(110)$ is a consequence of the equivalency of the two box states, one from each of the two cages in the unit cell of the sodalite unit cell.

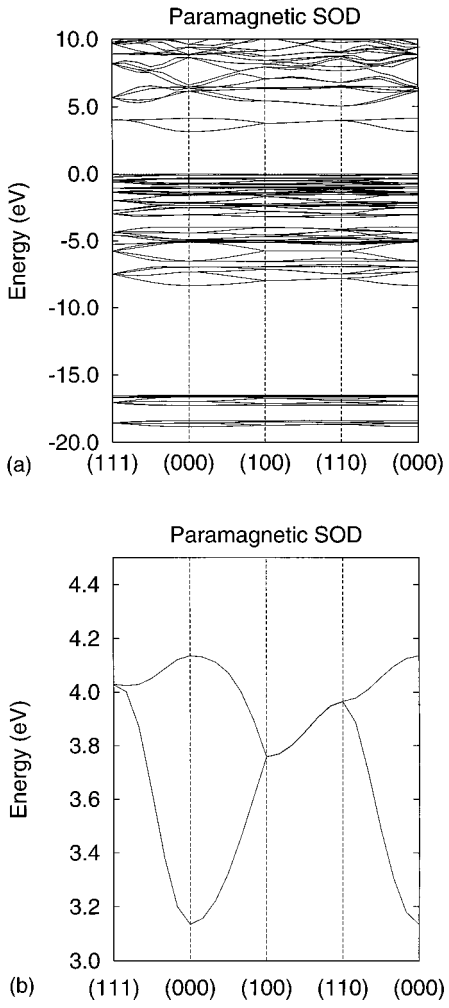

FIG. 5. Band structure of black sodalite, $Na_8(AlSiO_4)_6$, in the paramagnetic state obtained from non-spin-polarized LDA theory. (a) A plot of all of the low-lying bands. The valence-band maximum is defined to be at zero energy. The ''particle-in-a-box'' bands are those in the 3–4 eV range. Bands at 5 eV and above are conduction bands of the aluminosilicate. (b) A blowup of the ''particle-in-a-box'' bands induced by Na that lie in the aluminosilicate band gap. The Fermi level cuts through these bands near the center, and the system is predicted to be metallic.

The Fermi level will cut through this line and the system is metallic. Notice that the total width of the bands is about 0.9 eV, which can be used to estimate the hopping parameter t. In a nearest-neighbor model the bandwidth at the Γ point is $16t$, so $t \approx 0.06$ eV.

We now investigate the electronic structure of black sodalite allowing the spin system to polarize. The possible self-consistent polarization could be paramagnetic (no polarization), ferromagnetic, or antiferromagnetic. We make an initial guess for the charge density, which includes a slight spin polarization of the system. This breaks the symmetry. We then minimize the total energy by interacting to a self-consistent solution of the density-functional equations. After several iteration cycles, the minimum energy solution is found to be antiferromagnetic. Here one cage [say centered at (000)] has a net spin polarization up, while the second cage [centered at $(a/2)(111)$] has a net spin polarization down. The polarization is mainly due to a polarization of the

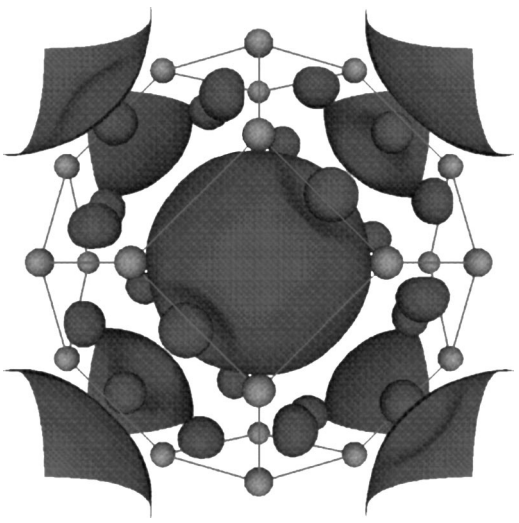

FIG. 6. A constant probability density contour for the Na-induced state at the Γ point of energy $\xi = 3.1$ eV [see Fig. 5(b)] of black sodalite. The β-cage framework of T atoms is superimposed as a ball-and-stick model. The large near-spherical density in the center of the β cage is the particle-in-a-box state, and the ''spherical blobs'' around the framework are probability density localized on the oxygen atoms. The eight ''wings'' on the outside of the cage are replicas of the central large near-spherical density in the centers of the neighboring cages along the eight (111) directions.

particle-in-a-box state. Figure 7 shows the polarization ξ in the (110) plane, which passes through the centers of the two cages (1 and 2) of the unit cell. We see that cage 1 has positive polarization and cage 2 has negative polarization corresponding to antiferromagnetic ordering. The energy difference between the spin-polarized and the non-spin-polarized system is very small, and is 0.030 eV per cell, while the total energy of the unit cell is $\approx -11\,500$ eV.

The band structure for the antiferromagnetic system is shown in Fig. 8(a), and is for spin up. The band structure for spin down is of course identical, but the spatial extent of the wave functions in the two cases is different. The k-dependent dispersion of the particle-in-a-box state lying near $+4.0$ eV

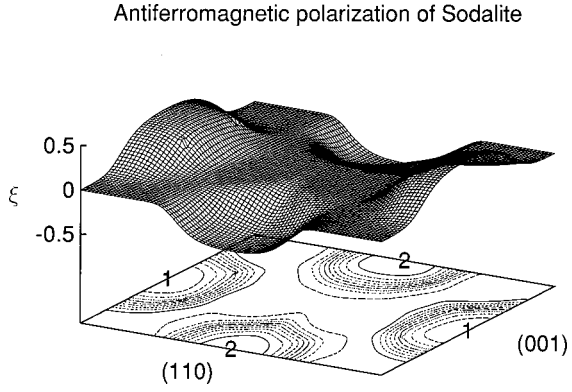

FIG. 7. Contour of spin polarization ξ in the $(\bar{1}10)$ plane, which passes through the centers of cages 1 and 2 at (000) and $(a/2)(111)$ in the unit cell, respectively. The cages ''1'' are polarized spin up, and the cages ''2'' are polarized spin down in an antiferromagnetic arrangement. The near-spherical spin density results from the polarization of the ''particle-in-a-spherical-box'' states.

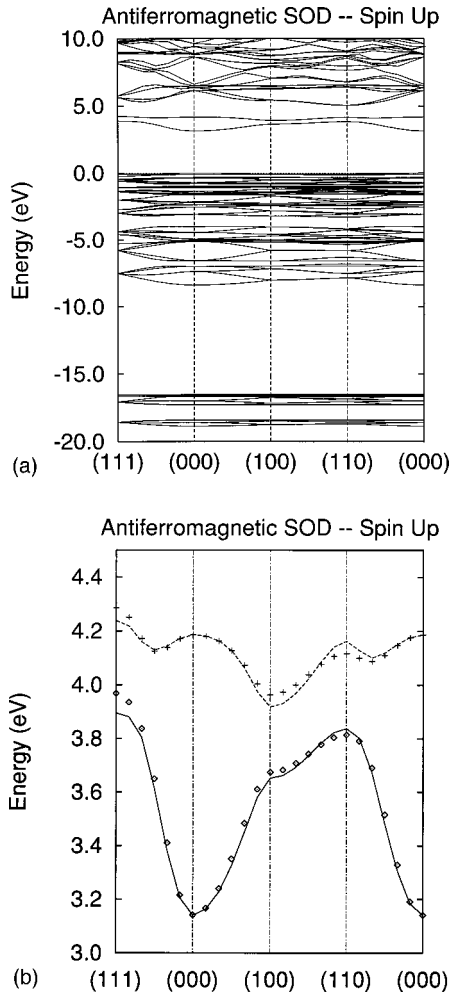

FIG. 8. Band structure of black sodalite, $Na_8(AlSiO_4)_6$, in the antiferromagnetic state obtained from LSDA functional theory. (a) All of the low-lying bands. The valence-band maximum is defined to be at zero energy. The ''particle-in-a-box'' bands occur near 4 eV. Bands at 5 eV and above are conduction bands. (b) A blowup of the ''particle-in-a-box'' bands in the band gap. At zero temperature the lowest band is occupied, and the upper band is unoccupied, forming a narrow gap antiferromagnetic insulator. The square and plus symbols are generated using a simple second-neighbor tight-binding model that is fit to the LSDA results.

is quite different from that of the paramagnetic system. There now exist small gaps at the Brillouin zone edges. (The minimum indirect gap between the bands is 23 meV; see below.) For example, a gap exists at the X point $[(\pi/a)(100)]$ of about 0.3 eV. This gap occurs because the two sodalite cages within the unit cell are no longer equivalent for a given spin. This inequivalency forces gaps to occur, and with the inclusion of spin *the system transforms from a paramagnetic metal to an antiferromagnetic insulator*.

A blow up view of the ''particle-in-a-box'' bands for the antiferromagnetic system is shown in Fig. 8(b) as solid lines. The lowest band is occupied with electrons and the upper band is empty (at zero temperature). The gap between the two bands is about 23 meV, which is very small and coincidentally roughly equal to the thermal energy at room temperature. The LSDA, however, is not accurate enough to draw a firm conclusion concerning the gap; however, the qualitative result that the system prefers antiferromagnetism and has a small gap (<0.3 eV) is probably reliable.

We can model the electronic structure of the antiferromagnetic system using a tight-binding approach. We assume each cage contains one s-like orbital, with the orbital ϕ_1 of the first cage at (000) having a self-energy of ϵ_1, and the orbital ϕ_2 of the second cage at $(\pi/a)(111)$ having a self-energy of ϵ_2. The overlap matrix between nearest-neighbor orbitals is S_1 and between second neighbors is S_2. There are eight first neighbors and a line connecting an atom with its first neighbor passes through a hexagonal face of a sodalite cage, while there are six second neighbors and a line connecting an atom with its second neighbor passes through a square face of a sodalite cage. Similarly the ''hopping'' (Hamiltonian) matrix elements between first neighbors, $\langle\phi_1|\hat{H}|\phi_2\rangle$, is $-t_1$, while the hopping matrix element between second neighbors is $-t_2$. We find by fitting to the LSDA results that $\epsilon_1=3.742$ eV, $\epsilon_2=4.039$ eV, $t_1=0.087$ eV, $t_2=-0.007$ eV, $S_1=-0.005$, and $S_2=0.011$. The results using the simple tight-binding model and the fit are shown as the symbols in Fig. 8(b). The fit is good, indicating that this simple physical picture is reasonable. The main physics when the spin is allowed to polarize differently in the two cages is that $\epsilon_1\neq\epsilon_2$, which means that the two ''noninteracting'' particle-in-a-box states from the two sodalite cages within the unit cell have different energies for a given spin. This energy difference is ≈ 0.3 eV (4.039–3.742) and accounts for the approximate 0.3 eV energy difference between the two states at $(a/2)(111)$, $(a/2)(110)$, and $(a/2)(000)$.

The small values of the hopping parameters just determined, or the hopping parameter of 0.06 eV estimated from the unpolarized band structure, indicate that $K/t\gg 1$ (using the estimate $K\approx 2$ eV of Sec. IV). Thus according to the analysis of Sec. IV, this should put us well into the antiferromagnetic regime. It is gratifying that the simple model and the self-consistent LSDA are in complete agreement on this point.

VI. CONSTRAINED PATH MONTE CARLO AND HARTREE-FOCK RESULTS

We have fit tight-binding parameters for the electronic band structure of sodalite in the paramagnetic state, obtained from non-spin-polarized LDA theory. A rough fit was given by $\epsilon_1=3.84$ eV, $t_1=0.0625$ eV, and $t_2=-0.03$ eV. These parameters are similar to the antiferromagnetic fit, with a somewhat greater second-neighbor coupling.

We propose to use either set of parameters within a Hubbard model Hamiltonian H describing the system:

$$H=-\sum_{(ij\sigma)} t_{ij}c^{\dagger}_{i\sigma}c_{j\sigma}+\sum_i Un_{i\uparrow}n_{i\downarrow}. \tag{11}$$

Here, $c^{\dagger}_{i\sigma}$ is the fermion operator that creates an electron of spin σ at site i, and t_{ij} is composed of ''hopping'' matrix elements. We define $n_{i\sigma}=c^{\dagger}_{i\sigma}c_{i\sigma}$, the number density of spin σ electrons at site i. We estimated U to be the Coulomb repulsion between two electrons in a spherical well of radius

$r_0 = 4.45$ Å, each with a wave function proportional to $j_0(r\pi/a)$. This integral was evaluated numerically, giving $U = 5.8$ eV.

To use the fitted parameters for the antiferromagnetic simulation, we ignore overlaps, setting $S_1 = S_2 = 0$. The energy splitting between ϵ_1 and ϵ_2 is a potential output rather than input of the calculation. As input, we use an average on-site energy $(\epsilon_1 + \epsilon_2)/2 = 3.8905$ eV. The number of electrons in black sodalite is equal to the number of cages available for occupation, thus the model is half-filled since each cage can potentially hold both one spin up and one spin down electron. Half-filled Hubbard models are generally thought to be antiferromagnetic.[45] Our sites form a bcc lattice with nearest-neighbor and second-neighbor couplings t_1 and t_2. Because t_2 is considerably smaller in magnitude than t_1, our first expectation is antiferromagnetic order with the two simple-cubic sublattices (body center and corner) having opposite spin. We performed Hartree-Fock and quantum Monte Carlo calculations that confirm this picture.

The Hartree-Fock solution of Eq. (11) is a single slater determinant wave function

$$|\Psi\rangle = \phi_1^\dagger \cdots \phi_n^\dagger |0\rangle, \tag{12}$$

where $|0\rangle$ is the zero-particle or vacuum state, and $\phi_i^\dagger = \Sigma_j \Phi_{ij} c_j^\dagger$ creates a particle in the single-particle orbital i that is a linear combination of local orbitals at site j. The Hartree-Fock solution is chosen to minimize the total energy. By the variational theorem it gives an upper bound on the ground-state energy. The error in this upper bound is the correlation energy; it is due to many-body correlations in the true ground state.

Our earlier estimates from density-functional theory indicated that the correlation energy is relatively small for this system, in comparison to the contribution due to exchange. For this reason, we would expect the quality of Hartree-Fock modeling to be excellent. Regardless of the tight-binding parameter set we use, we find an antiferromagnetic Hartree-Fock solution. For the tight-binding parameter set fit to the antiferromagnetic simulation, we find an average energy per site of 3.880 eV, and a moment per site $n_{i\uparrow} - n_{i\downarrow} = 0.9966$. For the other parameter set we find an average energy per site of 3.835 eV, and $n_{i\uparrow} - n_{i\downarrow} = 0.9982$. In each case the degree of antiferromagnetic ordering is nearly complete, with the two simple-cubic sublattices having opposite spin as expected. We used a $2\times2\times2$ simple cubic cell, with 16 lattice sites, for these calculations.

As an additional check, we performed quantum Monte Carlo (QMC) (Ref. 45) calculations using the recently developed constrained path Monte Carlo (CPMC) method.[46,47] For two-dimensional Hubbard models with a range of coupling parameters, this method recovers over 90% of the correlation energy. Briefly, the method works by evolving a trial wave function $|\Psi_T\rangle$ in imaginary time:

$$|\Psi\rangle = e^{-H\tau}|\Psi_T\rangle. \tag{13}$$

If τ is large, $|\Psi\rangle$ becomes an excellent approximation to the ground state, as the imaginary time propagator amplifies the lowest-energy components of $|\Psi_T\rangle$. In our case, the Hartree-Fock solution is used for $|\Psi_T\rangle$.

The imaginary time propagator is applied as follows:

$$e^{-H\tau} = \prod_{i=1}^{N} e^{-H\Delta\tau}, \tag{14}$$

where $\Delta\tau$ is a small time step, and

$$e^{-H\Delta\tau} \approx e^{-K\Delta\tau/2} e^{-V\Delta\tau} e^{-K\Delta\tau/2} \tag{15}$$

is the Trotter formula for the propagator, good to second order in $\Delta\tau$. $K = -\Sigma_{(ij\sigma)} t_{ij} c_{i\sigma}^\dagger c_{j\sigma}$ and $V = \Sigma_i U n_{i\uparrow} n_{i\downarrow}$ are the kinetic and potential energy contributions, respectively.

The propagator $\exp(-K\Delta\tau/2)$ acting on one Slater determinant gives another, and is easy to apply exactly. The potential energy gives a propagator $\exp(V\Delta\tau)$, which is more complicated to apply. It is first expanded as a product of terms $\exp(\Delta\tau U n_{i\uparrow} n_{i\downarrow})$. This term can be reexpressed using the discrete version of the Hubbard-Stratonovich transformation,

$$e^{-\Delta\tau U n_{i\uparrow} n_{i\downarrow}} = e^{-\Delta\tau U (n_{i\uparrow} + n_{i\downarrow})/2} \sum_{x_i = \pm 1} \frac{1}{2} e^{\gamma x_i (n_{i\uparrow} - n_{i\downarrow})}, \tag{16}$$

where $\cosh(\gamma) = \exp(\Delta\tau U/2)$. This equation can easily be verified for the four relevant cases $(n_{i,\uparrow}, n_{i,\downarrow}) = (0,0)$, $(0,1)$, $(1,0)$, and $(1,1)$. Each time such a term is encountered, one term in the summation is selected at random. The relative probability of selecting the two values for x_i is not equal. This weighting scheme and other necessary details of the method are discussed in Ref. 46.

Many such random walks are performed to sample the true, ground-state wave function. It is also necessary to further constrain the resulting random walkers $|\Phi\rangle$ by a condition $\langle \Phi_T | \Phi \rangle \geqslant 0$. Without this constraint, paths tend to add incoherently, causing computed properties to be dominated by noise.[46] Because of the constraint, the random walk gives an upper bound on the ground-state energy and does not converge to the true ground-state energy.

In our QMC calculations, we again find the system to be antiferromagnetic. For the tight-binding parameter set fit to the antiferromagnetic simulation, we find a moment per site $n_{i\uparrow} - n_{i\downarrow} = 0.9964 \pm 0.0001$. For the other parameter set we find $n_{i\uparrow} - n_{i\downarrow} = 0.9982 \pm 0.0001$. The correlation energy was very small. It is about 2.1×10^{-5} eV per electron and 6.7×10^{-6} eV per electron in the two cases, respectively.

These results can be better understood by the following transformation. It is known that the half-filled Hubbard model becomes isomorphic to the spin-1/2 Heisenberg antiferromagnet when U is large.[48] The Heisenberg model is defined by the Hamiltonian

$$H = \sum_{(ij)} J_{ij} S_i S_j. \tag{17}$$

The couplings $J_{ij} = 4t_{ij}^2/U$ replace the nearly forbidden hopping degrees of freedom of the electrons. The couplings result from a second-order perturbation treatment that removes the hopping. For the tight-binding parameter fits, $J = 0.003$ and 0.005 eV for the nearest-neighbor couplings of the paramagnetic and the antiferromagnetic fits, respectively. From this, the characteristic temperature scale for appearance of antiferromagnetism, $J/k_B = 30$ K or 50 K, can be deduced. This is in qualitative agreement with Srdanov *et al.*,[30] who find a transition temperature of 55 K.

VII. CONCLUSIONS

We have used an *ab initio* electronic-structure method to calculate the band structure of silica sodalite $(SiO_2)_{12}$ and black sodalite $Na_8(AlSiO_4)_6$. We find that the lowest few conduction bands of silica sodalite do not show any signature for particle-in-a-box states, but that black sodalite has states in the band gap that have particle-in-a-box character. These states begin about 1 eV below the ''true'' conduction band, and are metallic if spin polarization is neglected. When spin polarization is allowed within the LSDA approximation, the self-consistent charge density evolves into an insulating antiferromagnetic ground state.

A simple analytical model is developed for this system. Possible solutions of this model are paramagnetic, ferromagnetic, antiferromagnetic, and charge-density-wave states. An estimation of the parameters of the model from the LSDA calculation shows the antiferromagentic state to be the 0 K ground state.

Finally a Hubbard model is developed using both a constrained path Monte Carlo and a Hartree-Fock approach. Again estimates of the parameters are obtained from the LSDA results and simple approximations, and again antiferromagnetic order is found. The characteristic temperature scale for the appearance of the antiferromagnetic transitions is 30–50 K.

ACKNOWLEDGMENTS

We thank the National Science Foundation (Contract No. DMR 95-26274) and the ASU MRSEC (Contract No. DMR 9632635) for supporting this work. Professor Kevin Schmidt (ASU) was very helpful in instructing us on the subtleties of the Monte Carlo method and we are indebted to him. We thank Professor Srdanov for sharing his work before publication and for stimulating conversations. We thank Dr. Nick Blake for stimulating conversations, particularly concerning the local spin density approximation.

*Present address: Motorola Inc., 2200 West Broadway Rd., Mesa, AZ 85202.

[1] A. Dyer, Chem. Industry **7**, 241 (1984).
[2] V. N. Bogomolov, E. L. Lutsenko, V. P. Petranovskii, and S. V. Kholodkevich, Pis'ma Zh. Eksp. Teor. Fiz. **23**, 528 (1976) [JETP Lett. **23**, 483 (1976)]; V. N. Bogomolov, S. V. Kholodkevich, S. G. Romanov, and L. S. Agroskin, Solid State Commun. **47**, 181 (1983).
[3] G. A. Ozin, A. Kuperman, and A. Stein, Angew. Chem. Int. Ed. Engl. **28**, 359 (1989).
[4] G. D. Stucky and J. E. MacDougall, Science **247**, 669 (1990).
[5] G. A. Ozin, Adv. Mater. **4**, 612 (1992).
[6] A. A. Demkov and O. F. Sankey, Chem. Mater. **8**, 1793 (1996).
[7] A. A. Demkov and O. F. Sankey, *Access in Nanoporous Materials*, edited by T. J. Pinnavaia and M. F. Thorpe (Plenum Press, New York, 1995), p. 273.
[8] A. A. Demkov and O. F. Sankey, Phys. Rev. B **56**, 10 497 (1997).
[9] P. H. Kasai, J. Chem. Phys. **43**, 3322 (1965).
[10] J. A. Rabo, C. L. Angel, P. M. Kasai, and V. Shomaker, Discuss. Faraday Soc. **41**, 328 (1966).
[11] N. P. Blake and G. D. Stucky, J. Inclusion Phenom. Molec. Recognition Chem. **21**, 299 (1995).
[12] P. P Edwards, P. A. Anderson, and J. M. Thomas, Acc. Chem. Res. **29**, 23 (1996).
[13] Y. Nozue, T. Kodaira, and T. Goto, Phys. Rev. Lett. **68**, 3789 (1992).
[14] T. Kodaira, Y. Nozue, S. Ohwashi, N. Togashi, and O. Terosaki, Surf. Rev. Lett. **3**, 717 (1996).
[15] A. Z. Chowdhury and K. Nasu, J. Phys. Chem. Solids **56**, 1193 (1995).
[16] C. P. Ursenbach, P. N. Madden, I. Stich, and M. C. Payne, J. Phys. Chem. **99**, 6697 (1995).
[17] K. Huag, V. Srdanov, G. Stucky, and H. Metiu, J. Phys. Chem. **96**, 3495 (1992).
[18] V. Srdanov, K. Huag, H. Matiu, and G. D. Stucky, J. Phys. Chem. **96**, 9039 (1992).
[19] A. Monnier, V. Srdanov, and H. Metiu, J. Chem. Phys. **100**, 6944 (1994).
[20] N. P. Blake, V. I. Srdanov, G. D. Stucky, and H. Metiu, J. Phys. Chem. **99**, 2127 (1995).
[21] A. Trave, F. Buda, and A. Fasolino, Phys. Rev. Lett. **77**, 5405 (1996).
[22] A. A. Demkov, J. Ortega, O. F. Sankey, and M. P. Grumbach, Phys. Rev. B **52**, 1618 (1995).
[23] F. Filippone, F. Buda, S. Iarlori, G. Moretti, and P. Porta, J. Phys. Chem. **99**, 12 883 (1995).
[24] Y.-N. Xu, and W. Y. Ching, Phys. Rev. B **44**, 11 048 (1991).
[25] L. Canpana, A. Selloni, J. Weber, A. Pasquarelle, I. Papai, and A Goursot, Chem. Phys. Lett. **226**, 245 (1994).
[26] R. M. Wentzcovitch and L. Stixrude, Am. Mineral. **82**, 663 (1997).
[27] B. Wingler, V. Milman, and M. C. Payne, Miner. Mag. **59**, 589 (1995).
[28] J. Sauer, Chem. Rev. **89**, 199 (1989).
[29] J. C. White and A. C. Hess, J. Phys. Chem. **97**, 8703 (1993).
[30] V. I. Srdanov, G. D. Stucky, and G. Engelhardt, Phys. Rev. Lett. **80**, 2449 (1998).
[31] W. Meier, D. Olson, and Ch. Baerlocher, *Atlas of Zeolite Structure Types*, 4th ed. (Elsevier, London, 1996).
[32] R. M. Barrer and J. F. Cole, J. Phys. Chem. Solids **29**, 1755 (1968).
[33] J. B. A. F. Smeulders, M. A. Hefni, A. A. K. Klaasen, E. deBoer, U. Westphal, and G. Geismar, Zeolites **7**, 347 (1987).
[34] D. M. Bibby and M. P. Dale, Nature (London) **317**, 157 (1985).
[35] J. W. Richardson, J. J. Pluth, J. V. Smith, W. J. Dytrych, and D. M. Bibby, J. Chem. Phys. **92**, 243 (1988).
[36] L. Pauling, Z. Kristallogr. **74**, 213 (1930).
[37] Von J. Löns and H. Shulz, Acta Crystallogr. **23**, 434 (1967).
[38] V. Srdanov (private communication). The values corresponding to those in Table II given by Srdanov from x-ray data of black sodalite are Na at (xxx) with $x=0.1745$, and $(xyz)=(0.1396,0.4354,0.1448)$ for oxygen.
[39] L. Kleinman and D. M. Bylander, Phys. Rev. Lett. **48**, 1425 (1982).
[40] G. Kerker, J. Phys. C **13**, 189 (1980); N. Troullier and J. L. Martins, Phys. Rev. B **43**, 1993 (1991).
[41] R. W. Jansen and O. F. Sankey, Phys. Rev. B **36**, 6520 (1987).
[42] H. J. Monkhorst and J. D. Pack, Phys. Rev. B **13**, 5188 (1976).
[43] S. H. Vosko, L. Wilk, and M. Nusair, Can. J. Phys. **58**, 7200 (1980).

[44] D. M. Ceperley, Phys. Rev. B **18**, 3126 (1978); This was later parametrized by J. P. Perdew and A. Zunger, *ibid.* **23**, 5048 (1981).

[45] Reviewed by H. De Raedt and W. von der Linden, in *The Monte Carlo Method in Condensed Matter Physics*, edited by K. Binder (Springer-Verlag, Berlin, 1992).

[46] S. Zhang, J. Carlson, and J. E. Gubernatis, Phys. Rev. B **55**, 7464 (1997).

[47] S. Zhang, J. Carlson, and J. E. Gubernatis, Phys. Rev. Lett. **78**, 4486 (1997).

[48] A. B. Harris and R. V. Lang, Phys. Rev. **157**, 295 (1967).